Available online at www.sciencedirect.com
ScienceDirect
Journal of Solid State Chemistry 180 (2007) 2756–2762
JOURNAL OF SOLID STATE CHEMISTRY
www.elsevier.com/locate/jssc

Electronic structure and magnetic properties of Ce_5CuPb_3

V.H. Tran[a,*], M. Gamża[b], A. Ślebarski[b], J. Jarmulska[a], W. Miiller[a]

[a] *W. Trzebiatowski Institute of Low Temperature and Structure Research, Polish Academy of Sciences, P.O. Box 1410, 50-950 Wrocław, Poland*
[b] *Institute of Physics, University of Silesia, Uniwersytecka 4, 40-007 Katowice, Poland*

Received 25 May 2007; received in revised form 5 July 2007; accepted 8 July 2007
Available online 9 August 2007

Abstract

We report on the magnetic and electronic transport properties and as well band electronic structure of the Ce_5CuPb_3 intermetallic compound, crystallizing in the hexagonal Hf_5CuSn_3-type structure. The magnetic and XPS data indicate localized character of the 4*f*-electrons. Ce_5CuPb_3 is shown to be a magnet with double transitions below $T_{C1} = 46$ K and $T_{C2} = 5$ K. Despite being magnetic the compound is found to have a strongly enhanced electronic specific heat (about 50 mJ/mol Ce K^2). The electronic band structure calculations based on TB-LMTO and FP-LAPW confirm the magnetic ground state. From the theoretical data we would expect that the Ce1 and Ce2 atoms located at the 4*d* and 6*g*, respectively, give distinct contributions to the density of states at the Fermi level.

PACS: 71.27.+a; 71.20.Lp; 75.20.Hr; 75.30. −m

Keywords: 4*f*-intermetallics; Multiple magnetic phase transitions; *f-spd* hybridization

1. Introduction

The Ce-based intermetallic compounds present a variety of interesting phenomena, including both complex magnetic structures, intermediate valence Kondo lattice and heavy-fermion [1]. This rich magnetic behaviour emerges as a result of the delicate balance between two competing mechanisms: the oscillating Ruderman–Kittel–Kasuya–Yosida (RRKY) interaction and Kondo screening of the 4*f*-moments [2]. The first interaction brings about long-range magnetic order, while the latter suppresses the localized moments and may generate an Abrikosov–Suhl resonance close to the Fermi level. In recent investigations on the family of intermetallic compounds of the chemical formula $Ce_5Cu\mathit{M}_3$, where M = Sn and Sb and Bi [3–6], we have shown that these compounds may be classified as medium heavy fermion compounds since at low temperatures the Sommerfeld coefficient attains large values of the order of 200 mJ/mol Ce K^2. All the investigated compounds order magnetically at low temperatures.

In this work we investigate electronic structure and magnetic properties of Ce_5CuPb_3, as the isostructural compound to Ce_5CuSn_3. The presence of the Pb atoms as a ligand for the magnetic Ce ions enlarges the unit cell volume compared to that of Ce_5CuSn_3. This should lower the magnitude of the exchange parameter, which is usually responsible for the hybridization strength between the 4*f*-electrons and conduction electron band. In a consequence, one would expect the 4*f*-electrons in Ce_5CuPb_3 to be more localized than those in Ce_5CuSn_3.

Previously, Ce_5CuPb_3 and other ternary rare earth plumbites R_5CuPb_3 were reported by Gulay et al. [7] to crystallize in the hexagonal Hf_5CuSn_3-type structure (space group $P6_3/mcm$). These compounds are characterized by two different sites for the *R* ions, namely 4*d* and 6*g*, respectively. Amongst these materials, only Dy_5CuPb_3 has been studied so far as regards magnetic and electron transport properties [8]. It has been shown that in this alloy there are complex magnetic phase transitions, ferromagnetic below 45 K and ferrimagnetic below 6.5 K.

*Corresponding author. Fax: +48 71 344 1029.
E-mail address: V.H.Tran@int.pan.wroc.pl (V.H. Tran).

0022-4596/$ - see front matter © 2007 Elsevier Inc. All rights reserved.
doi:10.1016/j.jssc.2007.07.019

The magnetism of Dy_5CuPb_3 is believed due to the localized Dy^{3+} ions.

2. Experimental details

Several specimens of the ternary compound Ce_5CuPb_3 were prepared by arc-melting stoichiometric amounts of the high-purity elements (Ce 99.9 mass%, Cu 99.999 mass% and Pb 99.999 mass%) in a Ti-gettered pure argon atmosphere. The specimens were remelted several times to ensure homogeneity. After annealing at 800 °C for one week, the specimens were examined by X-ray powder diffraction at room temperature. The observed Bragg peaks can be indexed to the hexagonal structure with the space group $P6_3/mcm$. The refined lattice parameters are: $a = 9.551(2)$ Å and $c = 6.776(2)$ Å, and are comparable to those previously reported [7]. The composition of the obtained samples was established using an energy dispersive X-ray analysis with a Philips EDX515-PV9800 scanning electron microscope. It turns out that in addition to the major 513 phase, there exists a small quantity of free Pb metal. The data reported in this work were done on the sample, which contains a few percentage of the Pb contamination.

X-ray photoemission spectra were obtained with monochromatized AlKα radiation at room temperature using a PHI 5700/660 ESCA spectrometer. The spectra were collected immediately after breaking the samples in a vacuum of 10^{-10} Torr. The binding energies were referenced to the position of the gold 4*f*-level (84 eV), taken as the Fermi level. dc-Magnetization measurements were carried out with a Quantum Design SQUID magnetometer in fields up to 5.5 T and in the temperature range 2–400 K. Heat capacity was measured in the temperature range 2–100 K, utilizing a thermal relaxation method. Electrical resistivity was measured by the standard dc four-probe technique in the temperature range 4–300 K. The sample was rectangular with typical dimensions 0.5 mm × 0.5 mm × 5 mm. The voltage and current leads with Au-wires were attached using a silver paste. Thermoelectric power TEP was measured in the temperature range 4–300 K, using a differential method. The temperature and the corresponding voltage gradients across samples were recorded simultaneously using Fe–Au/Chromel thermocouples.

We have investigated the electronic structure of Ce_5CuPb_3 using both the scalar-relativistic tight-binding linear muffin-tin orbital (TB-LMTO) method [9] and the full-potential linear augmented plane wave (FP-LAPW) method [10,11]. In the calculations we used the experimental lattice parameters. In the first method, the crystal potential was used within the atomic sphere approximation (ASA) with overlapping Wigner–Seitz (W–S) spheres centred at atomic positions, filling up the unit cell volume. The total overlap volume was less than 9% of the unit cell volume. The exchange-correlation (EC) potential was included in the local spin-density approximation (LSDA) with the von Barth-Hedin parametrization [12]. The nonlocal corrections to the EC potential were taken into consideration in form proposed by Langreth–Mehl–Hu [13]. The self-consistent calculations were performed for the following *k*-mesh: 48 × 48 × 72 (8029 *k*-points in the irreducible wedge of the first Brillouin zone) to achieve a high accuracy in total energy. In the second method of calculations we have used the WIEN2k computer code [14] with the unit cell divided into non-overlapping atomic spheres (centred at the atomic sites) and the interstitial region. The muffin-tin radii were assumed to be 2.5 a.u. for all Ce, Cu and Pb. The EC potential was assumed within the generalized gradient approximation (GGA) in the form developed by Perdew et al. [15]. The Brillouin zone integrations were done over 40 *k*-points in the irreducible wedge (500 *k*-points in the full zone). The core levels were treated completely relativistically, while for valence states relativistic effects were included in a scalar relativistic treatment [16]. We have also optimized atomic positions basing on atomic forces within the nonmagnetic GGA approximation. The forces were calculated according to the method proposed by Yu et al. [17]. To investigate spin and orbital contributions to the total moments of Ce in two nonequivalent atomic positions, we performed spin-polarized calculations including spin–orbit interactions for valence states via a second variational step, using the scalar-relativistic eigenfunctions as basis [18].

3. Results and discussion

3.1. XPS results

The Ce 3*d* core level spectra of Ce_5CuPb_3 are shown in Fig. 1a. Roughly speaking the spectra consist of two peaks, separated by a spin–orbit coupling of $\Delta E = 18.6$ eV. These peaks correspond to the $3d_{5/2}$ and $3d_{3/2}$ doublet. Within the frameworks of single impurity model [19–21], we tried to explicate the Ce 4*f* electronic structure, making a deconvolution of these peaks. Since the $4f^0$ component cannot be detected in the experimental spectra, we do not take into account the $4f^0$ component. The fitted spectra for the $3d^9 4f^1$ and $3d^9 4f^2$ peaks are shown as solid lines. Due to the Coulomb interaction between an *f* electron and core-hole, the $3d^9 4f^2$ and $3d^9 4f^1$ peaks are moved one from other by an energy of about 1.1 eV. It can be seen that the intensity of the $3d^9 4f^2$ peak is quite small compared to that of $3d^9 4f^1$. The intensity ratio of the f^2 peak to the total 4*f* intensity is denoted by r_f, and has been reported to depend on the hybridization energy Δ [21]. For the Ce 3*d* spectra of Ce_5CuPb_3 we obtained $r_f = 0.066$, corresponding to the energy $\Delta = 35$ meV. Note that this value is comparable to those found in Ce compounds with the localized magnetic moments, such as in $CeAl_2$ and RPdAl [21].

The Ce 4*d* spectra of Ce_5CuPb_3 (Fig. 1b) can be decomposed into four components. The largest peaks would be built up by the two $4d_{5/2}$ and $4d_{3/2}$ lines separated by a spin–orbit coupling of 3.1 eV. However, due to multiplet interaction, one must bear in mind that it is hard to associate these components to single transitions, for instance, the peak

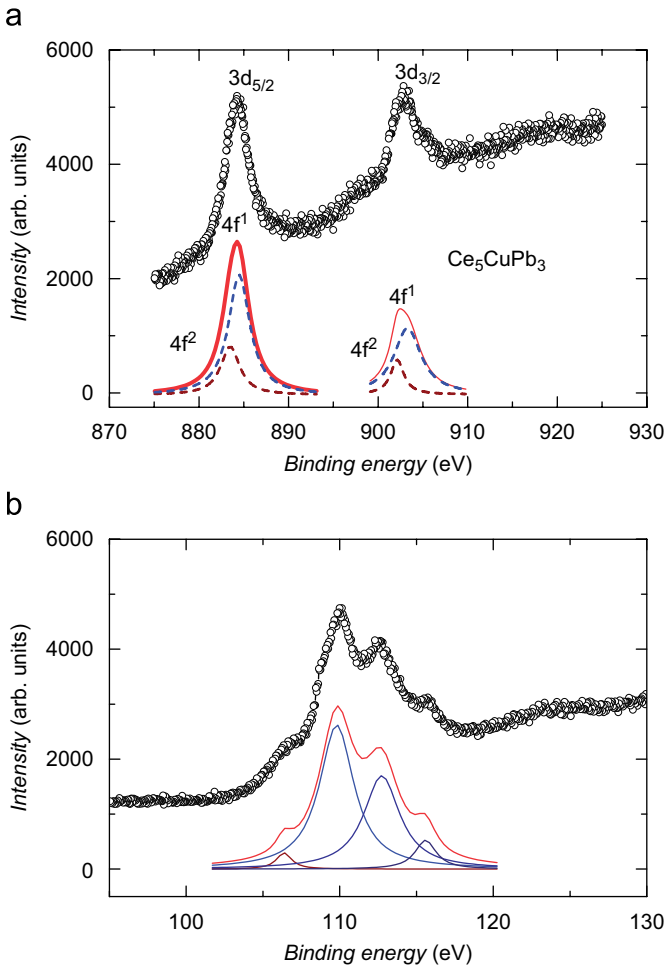

Fig. 1. Experimental and deconvoluted X-ray photoelectron spectra of (a) the Ce 3*d* core level and (b) the Ce 4*d* core level of Ce_5CuPb_3.

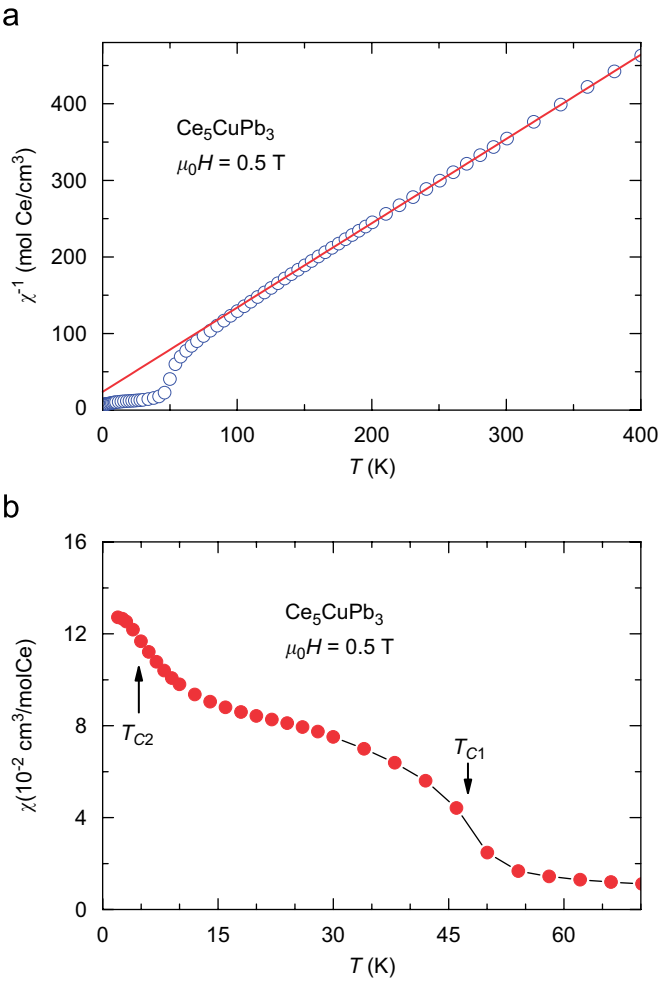

Fig. 2. (a) Temperature dependence of the inverse magnetic susceptibility of Ce_5CuPb_3 measured at 0.5 T. The solid line is the fit to the Curie–Weiss law. (b) Temperature dependence of the magnetic susceptibility of Ce_5CuPb_3. The arrows indicate magnetic phase transitions.

at binding energy of about 110 eV is certainly related to the Cu 3*s* emission as well. We notice that there is absence of the f^0 peak in the XPS Ce 4*d* spectra, thus ruling out the possibility of an intermediate valence system. This finding is consistent with the relatively low value of the hybridization energy of the 4*f*-electrons. We have collected also the valence XPS spectrum for Ce_5CuPb_3 and it will be compared with theoretical data shown in the next section.

3.2. Magnetic susceptibility and magnetization

The temperature dependence of the magnetic susceptibility of Ce_5CuPb_3 measured at a field of 0.5 T and in the temperature range 150–400 K (Fig. 2a) can be described by a Curie–Weiss law with an effective moment $\mu_{eff} = 2.69(2)\,\mu_B$ and a paramagnetic Curie temperature $\Theta_p = -21.8(5)$ K. The experimental value of μ_{eff} is close to the Russell-Saunders value for a free Ce^{3+} ion ($2.54\,\mu_B$), designating the localized character of the Ce 4*f*-electron. A negative value of Θ_p may indicate the existence of antiferromagnetic exchange interaction in the studied compound. At low temperatures, the susceptibility curve shows step-like increase (Fig. 2b), giving a clear evidence of the occurrence of magnetic phase transitions. Inspecting the temperature derivative of the susceptibility $d\chi(T)/dT$, one observes two minima at $T_{C1} = 46.0 \pm 0.5$ K and $T_{C2} = 5.0 \pm 0.5$ K indicated by arrows in Fig. 2b. Taking into account the substantial values of the susceptibility and the shape of the $d\chi(T)/dT$ curve we tentatively ascribe these anomalies to ferromagnetic-like transitions. In the same manner like Dy_5CuPb_3 [8], the double magnetic phase transition may be associated to two inequivalent magnetic sublattices of the magnetic Ce ions.

To further study the nature of the two phase transitions at T_{C1} and T_{C2} we measured magnetization at several selected temperatures below 75 K. The obtained data are shown in Fig. 3. For the data below T_{C2} we found that the initial magnetization is linear and it displays a metamagnetic-like transition, i.e., at about 1 T for the data at 2 K and at 0.5 T for those at 5 K. Moreover, these low-temperature data distinguish themselves by a hysteresis, which appears below ~1 T. These all observed features imply a ferri- or an antiferromagnetic character of the transition at T_{C2}. Fig. 3b presents magnetization data

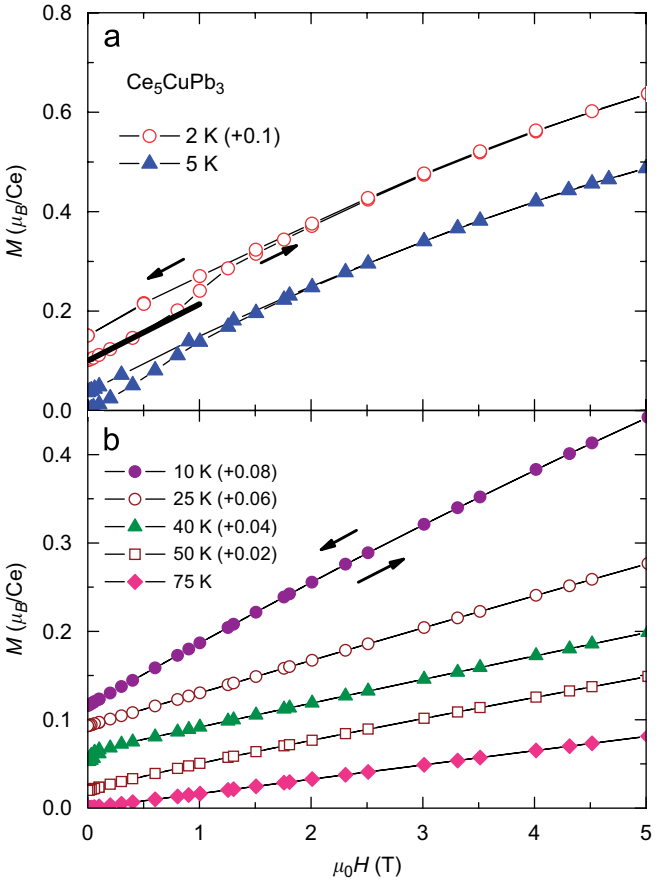

Fig. 3. Magnetization of Ce_5CuPb_3 measured at several temperatures below 75 K. For a clarity of presentation the data collected at 2, 10, 25, 40 and 50 K are shifted upwards by value given in the figure. The arrows indicate increasing or decreasing magnetic field strength. The solid line in the upper panel indicates an antiferromagnetic character of the transition T_{C2}. The arrows denote the data collected during the increasing and decreasing field strengths.

taken between 10 and 75 K. As can be seen the data collected at 10, 25 and 40 K, i.e., between T_{C2} and T_{C1}, show a spontaneous magnetization. Such a behaviour is consistent with the magnetic phase transition of the ferromagnetic origin at T_{C1}. However, it is noted that at the maximum strength of the applied magnetic field of 5 T, the magnetization attains rather a small value (0.36 μ_B) and does not saturate. This observation hints that only a part of the Ce ions undergoes a transition into the ferromagnetic state. Obviously, future neutron diffraction measurements are needed to confirm or reject this suggestion.

3.3. Specific heat

The temperature dependence of the specific heat of Ce_5CuPb_3 is displayed in Fig. 4. The data exhibit a clear lambda-like shape anomaly around 4 K. If the transition temperature is taken as the middle point of the specific heat jump we can estimate T_{C2} to be 5.2 K. This value is practically the same as determined from the magnetic measurement. The transition at T_{C1} in the $C_p(T)/T$ curve

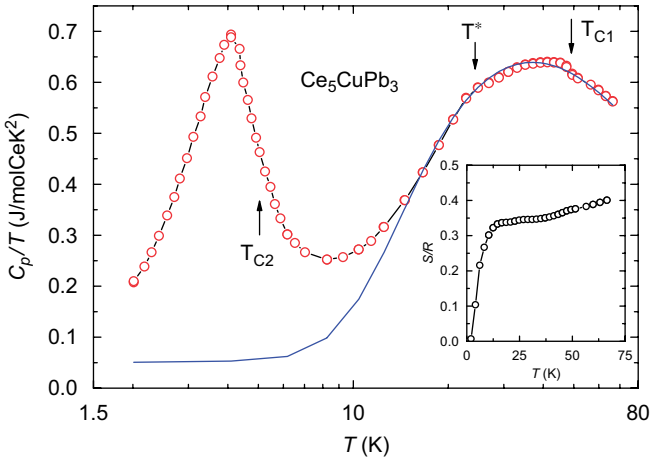

Fig. 4. Temperature dependence of the C_p/T ratio of Ce_5CuPb_3. The solid line is the sum of the lattice and electronic specific heat contributions. The inset shows the temperature dependence of the estimated magnetic entropy, $S = \int_0^{70\,K}(C_{mag}/T)\,dT$.

is less pronounced and amounts approximately to 49 K. The specific heat data do exhibit a kink at T^* of about 25 K. Unfortunately, the origin of this anomaly is unknown. We have attempted to look for reasons caused by eventual impurities like CeCuPb and Ce_5Pb_3, however, magnetic susceptibility of these compounds does not show any irregularity around neither T^* or T_{C1} and T_{C2}.

The phonon contribution to the total specific heat, C_{ph}, has assumed to follow the sum of the Debye $f(\Theta_D, T)$ and Einstein $f(\Theta_E, T)$ functions. The fit of the experimental data in the temperature range 20–100 K to the equation: $C_p = f(\Theta_D, T) + f(\Theta_E, T) + \gamma T$, where Θ_D and Θ_E are the Debye and Einstein temperatures, respectively, and $C_{el} = \gamma T$ is the electronic specific heat, yielded $\Theta_D = 218(2)$ K, $\Theta_E = 70(5)$ K and $\gamma = 50(2)$ mJ/mol Ce K^2. The Debye and Einstein vibrators are obtained as $n_D = 5$ and $n_E = 4$, respectively. We may add that the observed electronic specific heat of Ce_5CuPb_3 is typical as found in numbers of medium electron correlated Ce compounds. However, due to the low-temperature magnetic phase transition, the definitive γ value may be obtained at lower temperature range only.

If we tentatively accept the theoretical curve as the lattice and electronic contributions to the total specific heat we may estimate the magnetic specific heat as the difference: $C_{mag} = C_p - C_{ph} - C_{el}$. The estimated gain in the magnetic entropy, $S = \int_0^{70\,K}(C_{mag}/T)\,dT$, due to the magnetic orderings of the Ce ions becomes 3.1 J/mol Ce K at T_{C1} (inset of Fig. 4). The value is about 53% of the value Rln2 for a doublet ground state. We may admit that as far as the phonon reference is not available the estimated entropy must be taken with some caution.

3.4. Electronic transport properties

The temperature dependence of the electrical resistivity of Ce_5CuPb_3 measured in a low magnetic field of 0.05 T

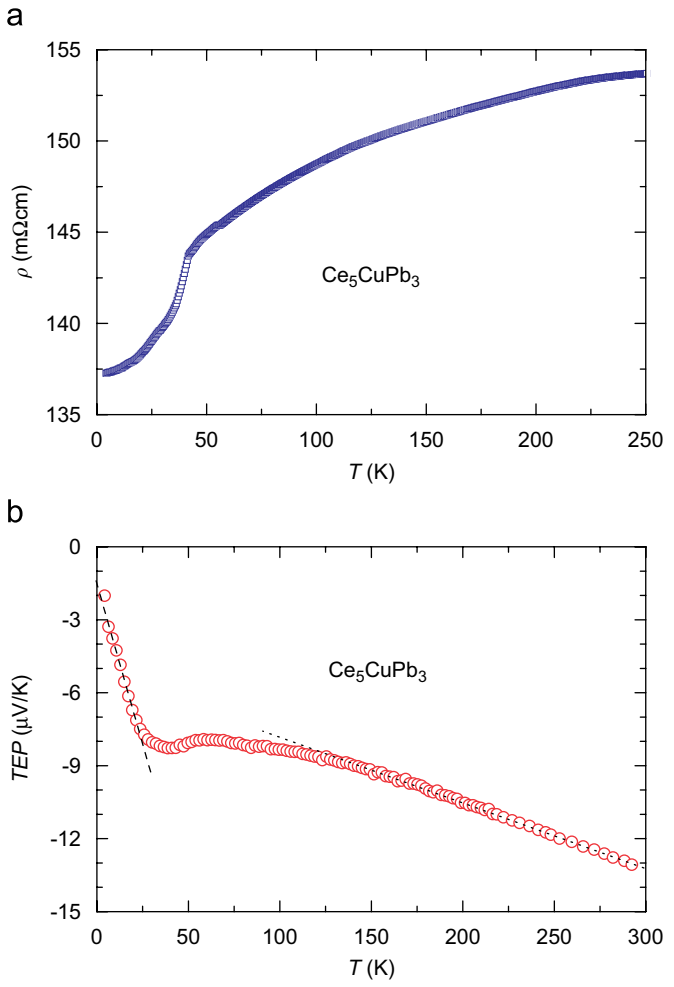

Fig. 5. (a) Temperature dependence of the electrical resistivity of Ce_5CuPb_3. (b) Temperature dependence of the thermoelectric power of Ce_5CuPb_3. The dashed and dotted lines are guides to the eye.

(Fig. 5a) displays a sharp decrease around T_{C1}. Such a decrease is usually ascribed to a reduction of the spin-disorder scattering. However, it is hard to gain information related to the transition at T_{C2}, since the resistivity measurements on several synthesized samples of Ce_5CuPb_3 at zero field have shown systematic presence of a severe drop in the resistivity at 6.5 K, due to the superconductivity of free lead in the samples. It should be added that the superconducting phenomenon in Ce_5CuPb_3 can be eliminated by measurements in a magnetic field of about 0.05 T. Because of micro-cracks and the oxidation problem, the geometric dimension cannot be exactly determined, we advice to take the absolute values of the measured resistivity with great caution. The magnetoresistance measured in fields up to 8 T (not shown here) has rather small values, for instance, at 10 K $\Delta\rho/\rho$ amounts only to -2%.

The thermoelectric power of Ce_5CuPb_3 (Fig. 5b) is negative and reaches a value of $-13\,\mu V/K$ at room temperature. The thermopower displays two temperature ranges with the linear temperature dependence. Such a linear T-behaviour implies a dominating diffusion contribution. The change of the slope $S(T)/T$ in the crossover temperature range (30–100 K), nearby magnetic phase transition at $T_{C1} = 46$ K, suggests change in the Fermi level accompanied with the change in the carrier concentration.

3.5. Electronic band structure calculation

For the studied compound we first did the calculations for a nonmagnetic ground state by optimizing each coordinate of the atoms. We got total forces on atoms smaller than 1 mRy/a.u. for the following atomic positions: Ce1 ($\frac{1}{3}$, $\frac{2}{3}$, 0), Ce2 (0.2539, 0, $\frac{1}{4}$), Cu (0, 0, 0) and Pb (0.6127, 0, $\frac{1}{4}$). These values are roughly consistent with those deduced from the X-ray-powder diffraction patterns. Obviously, further X-ray-single crystal diffraction study is highly desired to support the theoretical results.

Band structure calculations for Ce_5CuPb_3 were performed assuming the nonmagnetic ground state as well as ferromagnetic and antiferromagnetic coupling between the Ce1 and Ce2 sublattices. Our calculations suggest that the ground state is magnetic and the lowest total energy was found for a simple ferromagnetic configuration with spins aligned collinearly along the z-axis. Figs. 6 and 7 display the spin-resolved total and partial atom-projected densities of states (DOS) for Ce_5CuPb_3 obtained within the TB-LMTO method for the above structure. The most characteristic feature of the DOS is the presence of narrow bands formed mainly by the Ce 4f states near the Fermi level. Such an electronic structure may imply a significant contribution of the 4f states to the electronic specific heat. However, carefully looking at the DOS one recognizes that the Fermi level is located inside a band pseudogap, as illustrated in inset of Fig. 6. This feature leads the DOS(E_F) to have a value of about 29.36 states/(eV f.u.), corresponding to an electronic specific heat coefficient of 69.2 mJ/mol K^2($\sim$14 mJ/mol Ce K^2). The latter value is consistent with the experimental one (50 mJ/mol Ce K^2), if bearing in mind that different kinds of interactions, e.g.

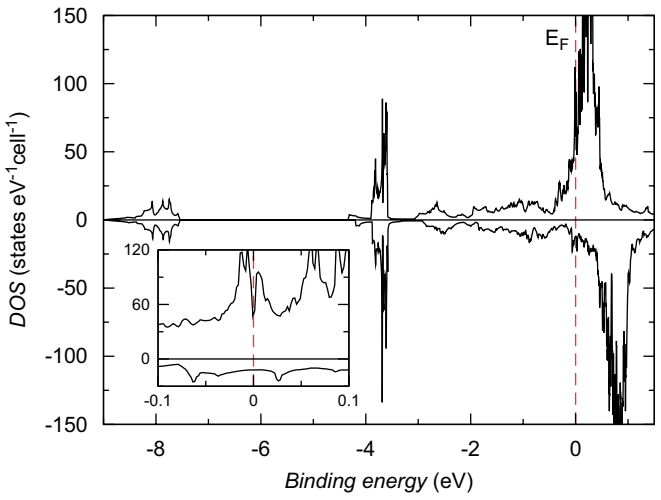

Fig. 6. Spin-projected total DOSs for ferromagnetic Ce_5CuPb_3 calculated within the TB-LMTO method. The inset shows the shape of DOSs near the Fermi level.

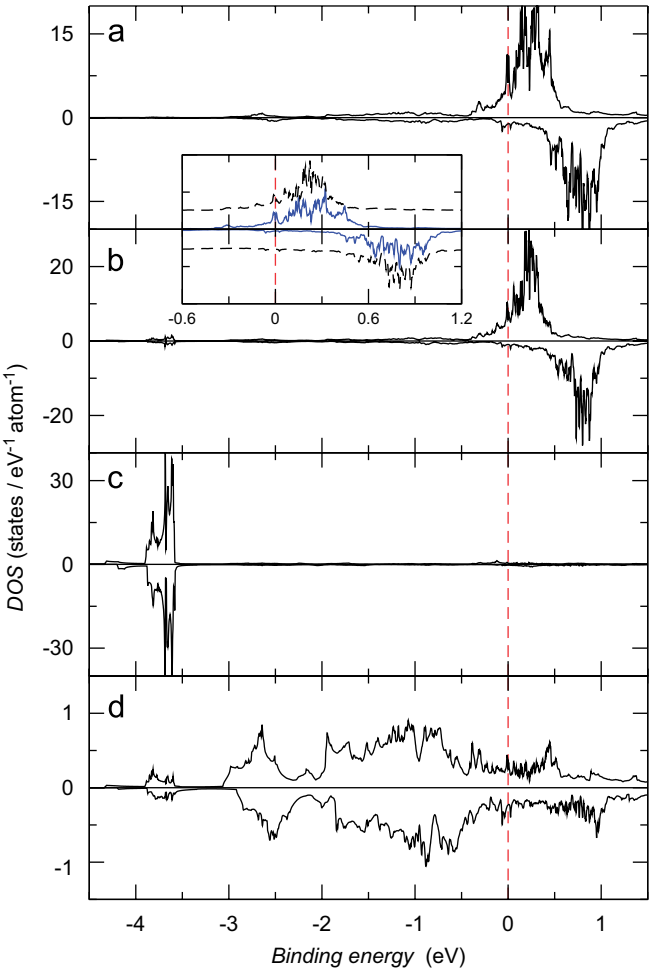

Fig. 7. Partial atom-spin projected DOSs for (a) Ce1, (b) Ce2, (c) Cu and (d) Pb obtained within the TB-LMTO method. The inset shows the comparison between the Ce1 (solid lines) and Ce2 (dashed lines) bands.

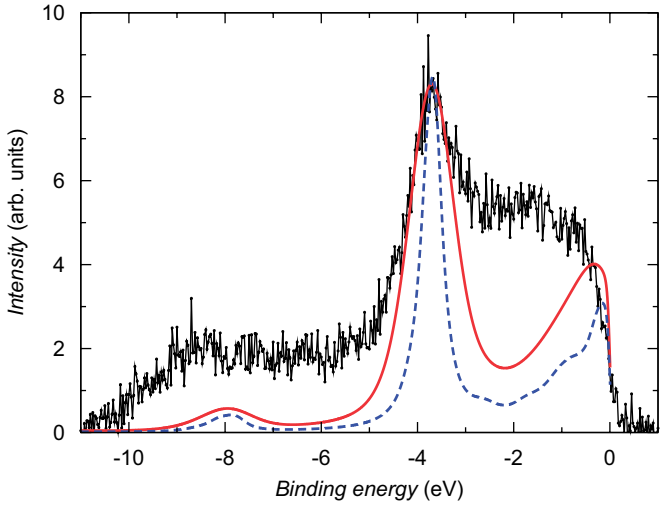

Fig. 8. Comparison of the experimental valence band corrected by the background (thin line with crosses) with the theoretical spectra. These latter were obtained by the multiplication of the partial l-resolved DOSs by the corresponding cross sections and then the data were convoluted by Lorentzians with a full-width-half-maximum (FWHM) of 0.4 eV (dashed line) or by the pseudoVoigt profile function with a FWHM of 0.8 and 0.5 eV for the Lorentzian and Gaussian components, respectively (solid line).

phonon-electron coupling and magnetic excitations usually result in an enhancement of experimental γ-value.

The inset of Fig. 7 shows a comparison of the partial DOSs of the Ce1 and Ce2 atoms. The Ce1 bands are more dispersive compared to those of Ce2. This observation hints that the Ce atoms at the nonequivalent 4*d* and 6*g* sites may do not contribute equally to the DOS(E_F) and they do not have equal magnetic moment. In fact, our band structure calculations reveal that the spin moments on the Ce1 and Ce2 atoms may have value of 0.976 and 0.983 μ_B, respectively. The theoretical spin moments on the Cu and Pb atoms were found to be less than 0.1 μ_B, manifesting that Cu and Pb practically do not carry any magnetic moment. In terms of the spin-polarized calculations with spin–orbit coupling we obtain spin μ_S and orbital [μ_L] moments at the Ce1 and Ce2 atoms to amount to 1.03[−0.46] and 0.90 [−0.71] μ_B, respectively. Thus, the total magnetic moments for Ce at the 4d position is equal to 0.57 μ_B, while for Ce at the 6*g* site only 0.19 μ_B.

The valence band spectra are shown in Fig. 8. A background of the spectra, calculated by means of a Tougaard algorithm [23], was subtracted from the experimental XPS data. We interpret the peak located at about 7.5–9 eV as originated from the Pb 6*s* states hybridized with the Ce bands (*spd*). The main peak visible in the XPS valence band is located at about 3.8 eV. This peak can be attributed to the Cu 3*d* states hybridized with the Ce2 and Pb bands. It is worthwhile to note that the energy position of the Cu 3*d* structure is little bit moved away from the Fermi level, if one compares to that of the pure Cu the 3*d* bands situated at about 3 eV. Such a shift may suggest a weak hybridization between the Ce and Cu electron bands. In other words, the 3*d* band is completely filled and it must be shifted to lower energies respect to the E_F. This situation conforms a localized character of the trivalent Ce ions. In Fig. 8 we compare the experimental spectra with those resulting from the band structure calculations. To simulate the theoretical valence band structure we have multiplied the partial l-resolved DOSs by the corresponding photo-ionization cross sections [22]. The data were then convoluted by Lorentzians with an FWHM of 0.4 eV in order to account the instrumental broadening. A comparison of the theoretical with experimental spectra has shown a good agreement regarding the peak positions. However, the peaks in the experimental data are significantly wider, probably due to some influence of the phonon broadening, the effect of lifetime of the hole states as well as due to impurities on the sample surface. Attempt to simulate spectra with the pseudoVoigt profile function with a FWHM of 0.8 and 0.5 eV for the Lorentzian and Gaussian components, respectively, seems to give a better agreement with the experimental resolution. The result of such simulation is shown in Fig. 8 as the solid line. We obtain an agreement regarding the positions of main peaks. The

disagreement in the magnitude could be partially originated from the small amount of oxygen and carbon compounds detected in the total XPS spectrum. Nevertheless, one must take into account the weakness of the used calculation method. We must admit that in the frameworks of the standard density functional theory based on the LSDA approximation, the 4*f* states cannot be adequately described. We believe that further theoretical band structure studies, notably these including strong correlations within the 4*f* states, for instance, so-called LSDA + U approximation [24] will give a more insight on the present discrepancy between the theoretical and the observed valence band.

4. Concluding remarks

We have measured XPS spectra, magnetization, specific heat, electrical resistivity, magnetoresistance and thermoelectric power of polycrystalline samples of Ce-based intermetallic compound Ce_5CuPb_3. We have carried out electronic band structure calculations. Combining with the previous reported data for isostructural compound [3], the present results indicate clear influence of the ligands on the magnetic properties of investigated compounds. The fact that the Ce_5CuSn_3 compound has been found to have larger electronic specific heat compared to that of Ce_5CuPb_3 may designate a more localized character of the Ce 4*f*-electrons in the latter compound. This behaviour can be anticipated from the change in the unit cell volume, which increases from Sn- to Pb-based compound. The increasing of the distance between the magnetic central and nonmagnetic ligand ions is presumably the main factor that weakens the hybridization between 4*f* and conduction electrons, and in consequence strengthens the localized electron magnetism.

The experimental data presented here indicate two successive magnetic phase transitions at $T_{C1} = 46.0 \pm 0.5\,\mathrm{K}$ and $T_{C2} = 5.0 \pm 0.5\,\mathrm{K}$. The multiple transitions are presumably caused by Ce–Ce exchange interactions in two nonequivalent Ce sites. One of the more important results of our study is the observation of different contribution of the Ce1 and Ce2 atoms to the physical properties. These magnetic Ce ions not only possess distinct magnetic moment values but they probably also contribute not equally to the DOS(E_F). The fact of disproportion of the ratio μ_S/μ_L between the Ce atoms suggests the presence of the Kondo screening most probably at the 6*g* site. This effect is undoubtedly is one of the reasons caused an enhancement in the electronic specific heat at low temperatures.

Acknowledgments

The authors would like to thank the Ministry of Science and Higher Education for the financial support; two of us (VHT and WM) within Grant no. N202 082 31/0449, AŚ within Grant no. 1 P03B 052 28 and MG within Grant no. N202 010 32/0487.

References

[1] F. Steglich, S. Süllow, Encyclopedia of Materials: Science and Technology, Elsevier, Amsterdam, 2001, p. 3746.
[2] S. Doniach, Valence Instabilities and Related Narrow Band Phenomena, in: R.D. Parks (Ed.), Plenum, New York, 1977, p. 169.
[3] V.H. Tran, J. Alloys Compds. 383 (2004) 281.
[4] V.H. Tran, Czech. J. Phys. 54 (2004) D411.
[5] V.H. Tran, Phys. Rev. B 70 (2004) 094424.
[6] V.H. Tran, M. Gamża, A. Ślebarski, J. Jarmulska, W. Miiller, J. Alloy Compds., in press, doi:10.1016/jallcom.2007.04.227.
[7] L.D. Gulay, J. Stępień-Damm, M. Wołcyrz, J. Alloys Compds. 319 (2001) 148.
[8] V.H. Tran, L.D. Gulay, J. Solid State Chem. 179 (2006) 646.
[9] O.K. Andersen, O. Jepsen, Phys. Rev. Lett. 53 (1984) 2571;
O.K. Andersen, O. Jepsen, D. Glötzel, in: F. Bassani, F. Fumi (Eds.), Highlights of Condensed Matter Theory, North-Holland, Amsterdam, 1985, p. 59;
O. Jepsen, O.K. Andersen, Solid State Commun. 9 (1971) 1763;
O.K. Andersen, O. Jepsen, M. Sob, in: M. Yussouff (Ed.), Electronic Band Structure and its Applications, Springer Lecture Notes in Physics, vol. 283, Springer, Berlin, 1987, p. 1.
[10] O.K. Andersen, Solid State Commun. 13 (1973) 133;
O.K. Andersen, Phys. Rev. B 12 (1975) 3060.
[11] D. Singh, Plane Waves, pseudopotentials and the LAPW Method, Kluwer Academic, 1994.
[12] V. von Barth, L. Hedin, J. Phys. C Solid State Phys. 5 (1972) 1629.
[13] C.D. Hu, D.C. Langreth, Phys. Scr. 32 (1985) 391.
[14] P. Blaha, K. Schwarz , G. Madsen , D. Kvasnicka , J. Luitz, Program for Calculating Crystal Properties, WIEN2k, Vienna University of Technology, 2001 (ISBN 3-9501031-1-2).
[15] J.P. Pardew, K. Burke, M. Ernzerhof, Phys. Rev. Lett. 77 (1996) 3865.
[16] D.D. Koelling, B.N. Harmon, J. Phys. C Solid State Phys. 10 (1977) 3107.
[17] R. Yu, D. Singh, H. Krakauer, Phys. Rev. B 43 (1991) 6411.
[18] A.H. MacDonald, W.E. Pickett, D.D. Koelling, J. Phys. C 13 (1980) 2675.
[19] O. Gunnarsson, K. Schönhammer, Phys. Rev. B 28 (1983) 4315.
[20] J.C. Fuggle, F.U. Hillebrecht, R. Zeller, Z. Zołnierek, P.A. Bennett, Ch. Freiburg, Phys. Rev. B 27 (1982) 2145.
[21] J.C. Fuggle, F.U. Hillebrecht, Z. Zołnierek, R. Lösser, Ch. Freiburg, O. Gunnarsson, K. Schönhammer, Phys. Rev. B 27 (1983) 7330.
[22] J.J. Yeh, J. Lindau, Data Nucl. Data Tables 32 (1985) 1.
[23] S. Tougaard, P. Sigmund, Phys. Rev. B 25 (1982) 4452.
[24] V.I. Anisimov, I.V. Solovyev, M.A. Korotin, M.T. Czyżyk, G.A. Sawatzky, Phys. Rev. B 48 (1993) 16929;
V.I. Anisimov, J. Zaanen, O.K. Andersen, Phys. Rev. B 44 (1991) 943;
V.I. Anisimov, F. Aryasetiawan, A.I. Lichtenstein, J. Phys. Condens. Matter 9 (1997) 767.